ADVANCED OPTICAL MATERIALS
www.advopticalmat.de

TADF Host Engineering for Improved Pure Blue Matrix-Free Hyperfluorescent OLEDs with Ultranarrow Emission

Hwan-Hee Cho, Daniel G. Congrave,* Sebastian Gorgon, Victor Riesgo-Gonzalez, Richard H. Friend,* and Hugo Bronstein**

Hyperfluorescence has been proposed as a promising approach for simultaneously efficient and stable blue electroluminescence. Two-component matrix-free hyperfluorescence (MFHF) is particularly appealing to simplify device fabrication but is limited by the availability of suitable blue thermally activated delayed fluorescent (TADF) hosts. In this work, blue TADF materials are developed with high non-doped OLED performance and apply them as hosts in MFHF devices. High maximum external quantum efficiencies (EQEs) of up to 23.2% are achieved from blue non-doped TADF organic light emitting diodes (OLEDs), facilitating efficient MFHF devices with ultranarrow pure blue emission (EQE > 20%, $CIE_y \approx 0.15$ and full-width at half-maximum ≤15 nm) upon incorporation of a narrowband terminal emitter with multi-resonance spectral features. Steady-state and transient photophysical studies support the high performance of non-doped TADF and MFHF OLEDs. Our results indicate that optimizing TADF hosts for intrinsic non-doped device efficiency is a viable direction to realize high-performing pure blue MFHF OLEDs based on a simple host-guest emissive system.

1. Introduction

Since the first organic electroluminescent device was introduced in 1987, a wide range of research into organic light-emitting diodes (OLEDs) has been conducted in academia and industry.[1] Harvesting triplet excitons by phosphorescent heavy metal complexes led to the dramatic improvement of OLED performance, especially for green and red OLEDs.[2,3] All-organic thermally activated delayed fluorescence (TADF) materials with almost 100% internal quantum efficiency (IQE) were next reported as a promising concept to surpass phosphorescent dopants.[4,5] Nevertheless, achieving stable and efficient blue electroluminescence is a persistent challenge.

In 2014, it was suggested that a TADF material could be adopted as a triplet harvesting exciton donor to a fluorescent acceptor (terminal emitter) to achieve high efficiency and stability simultaneously for the next generation of OLEDs.[6] Such a concept is quite promising since, alongside the high efficiency afforded by TADF, there is the potential for higher operational stability by accelerating the rate of triplet harvesting through energy transfer to a stable terminal emitter. The narrow full width at half maximum (FWHM) of rigid terminal emitters is also beneficial for color purity and minimizing the exciton energy required for pure blue emission. Consequently, there have been a variety of studies on this concept, so-called hyperfluorescence (HF), utilizing diverse combinations of TADF sensitizers and terminal emitters to afford almost 100% IQE.[7–18]

The emissive layer (EML) of a typical HF device consists of a wide gap matrix doped with a TADF sensitizer and fluorescent terminal emitter. Diluting the sensitizer and terminal emitter into a matrix offers a strategy to achieve high efficiency by suppressing concentration quenching, and modulating energy transfer to ensure that Förster resonance energy transfer (FRET) from the sensitizer to the terminal emitter is a dominant mechanism. However, a three-component (or even four if mixed matrices are used) EML increases the complexity and cost of device fabrication compared to a simple two-component EML, and popular high-gap matrices for deep blue TADF and HF OLEDs, such as DPEPO, are highly unstable under device operation.[19]

H.-H. Cho, S. Gorgon, R. H. Friend, H. Bronstein
Cavendish Laboratory
Department of Physics
University of Cambridge
J J Thomson Avenue, Cambridge CB3 0HE, UK
E-mail: chohh@yonsei.ac.kr; rhf10@cam.ac.uk; hab60@cam.ac.uk
H.-H. Cho
Department of Materials Science and Engineering
Yonsei University
50 Yonsei-ro, Seodaemun-gu, Seoul 03722, Republic of Korea
D. G. Congrave, H. Bronstein
Department of Chemistry
University of Cambridge
Cambridge CB2 1EW, UK
E-mail: dan.congrave@chem.ox.ac.uk
D. G. Congrave, V. Riesgo-Gonzalez
Department of Chemistry
University of Oxford
Chemistry Research Laboratory
Oxford OX1 3TA, UK

The ORCID identification number(s) for the author(s) of this article can be found under https://doi.org/10.1002/adom.202500246

DOI: 10.1002/adom.202500246

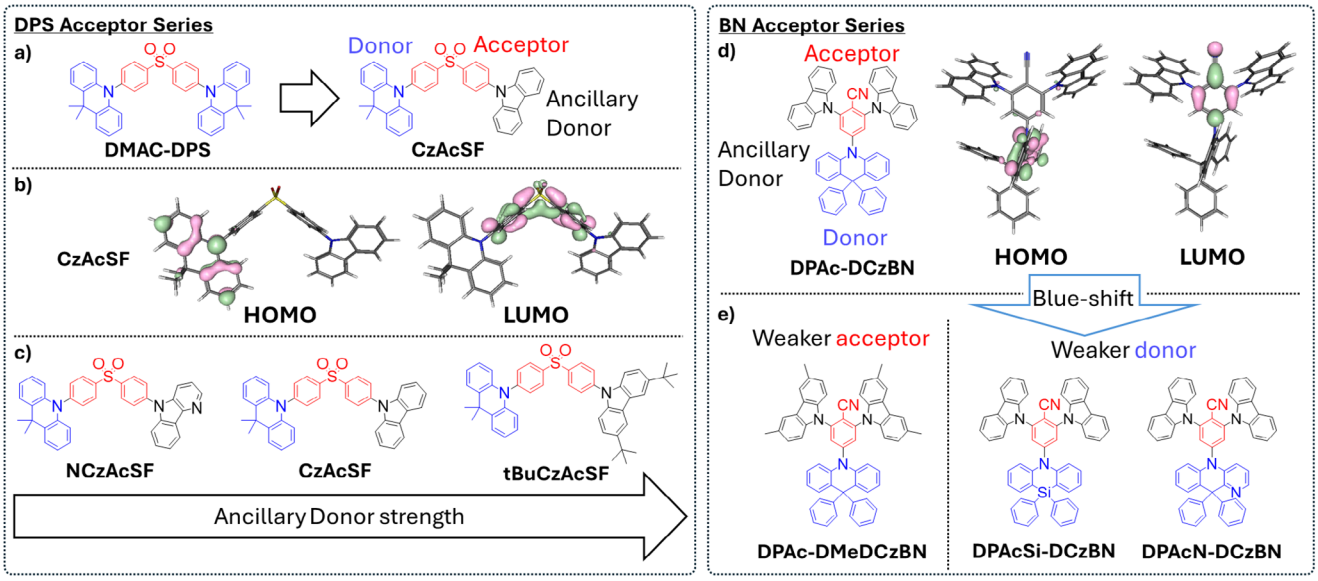

Figure 1. Design strategies for the new TADF hosts. a) Structures of **DMAC-DPS** and **CzAcSF**; b) HOMO and LUMO orbitals of **CzAcSF** (PBE0/def2svp); c) Structures of the DPS acceptor series molecules; d) Structure and HOMO and LUMO orbitals (PBE0/def2svp) of **DPAc-DCzBN**; e) Structures of the BN acceptor series molecules.

Utilizing simple two-component "matrix-free" hyperfluorescent (MFHF) EMLs is an appealing approach to overcome the limitations of matrix-containing devices.[18,20,21] In an MFHF device the TADF sensitizer functions as the host, and so must be able to efficiently harvest triplets in the neat film state (non-doped). A wide range of non-doped TADF materials has been reported that emit with high external quantum efficiency (EQE) across the visible spectrum.[22–25] For blue MFHF the TADF host must exhibit neat film emission sufficiently high in energy for energy transfer to a BT.2020-compatible blue multi-resonance terminal emitter, while also displaying a high non-doped EQE. Marrying high energy and efficiency in non-doped TADF materials in this manner has been highly challenging, which has limited efficient blue MFHF to a few select examples.[26,27] For blue MFHF to live up to its potential there is an urgent requirement to develop new high-energy and high-performing TADF hosts.

In this work, we have designed new TADF hosts with the aim of improving the efficiency and chromaticity coordinates of blue MFHF devices. A systematic series of high-performing non-doped blue TADF materials was developed. Non-doped blue TADF OLEDs fabricated from the new materials exhibit high maximum EQEs of up to 23.2% at a peak wavelength of 469 nm. On the basis of the non-doped TADF device results, the two best-performing TADF hosts were applied to MFHF systems. Upon doping the TADF hosts with a narrowband emitter with multi-resonance spectral features maximum EQEs of up to 22.2% were achieved with pure blue emission of FWHM $\leq$ 15 nm and CIE_y $\approx$0.15 at a peak wavelength of 456 nm, which are exceptional for MFHF devices incorporating a fluorescent terminal emitter. Steady-state and transient photophysical studies support efficient non-doped TADF characteristics and effective energy transfer, explaining the high performances of the non-doped TADF and MFHF OLEDs.

2. Results and Discussion

2.1. Design

We have recently reported that **DMAC-DPS**[28] and **DPAc-DCzBN**[29] (**Figure 1**) can serve as promising TADF hosts for blue MFHF devices.[20] However, despite the incorporation of BT.2020 terminal emitters with intrinsic CIE_y coordinates $\leq$ 0.05, the best CIE_y value that could be obtained from an MFHF device was 0.18 due to incomplete energy transfer from the TADF host. The aim of this work was to blue-shift the neat-film emission of **DMAC-DPS** and **DPAc-DCzBN** to improve energy transfer while retaining/improving their high non-doped OLED performance ($\geq$ 20% EQE). Hence, we sought to colour-tune the TADF hosts while minimizing any alterations to steric factors that influence intermolecular interactions in the neat film.

The molecular design strategies employed in this work are illustrated in Figure 1. Breaking the molecular symmetry of **DMAC-DPS** affords **CzAcSF**[26] (Figure 1a). The lowest energy charge transfer state consists of a transition between the primary 9,9-dimethylacridine (DMAC) donor and the diphenylsulfone (DPS) acceptor, i.e., a HOMO → LUMO transition (Figure 1b). The carbazole moiety functions as an ancillary donor, which we envisaged could be modified to alter the acceptor strength and so tune the emission wavelength (Figure 1c). The ancillary donor could be easily altered through exploiting the orthogonality of Buchwald-Hartwig and nucleophilic aromatic substitution (S_NAr) chemistry (synthetic details are included in the Supporting Information) to afford **CzAcSF**, **NCzAcSF**, and **tBuCzAcSF**, which constitute the DPS acceptor series.

DPAc-DCzBN can be treated in an analogous fashion to **CzAcSF**, where the 9,9-diphenylacridine (DPAC), benzonitrile (BN) and carbazole groups function as the primary donor, acceptor, and ancillary donor, respectively (Figure 1d). Here we aimed

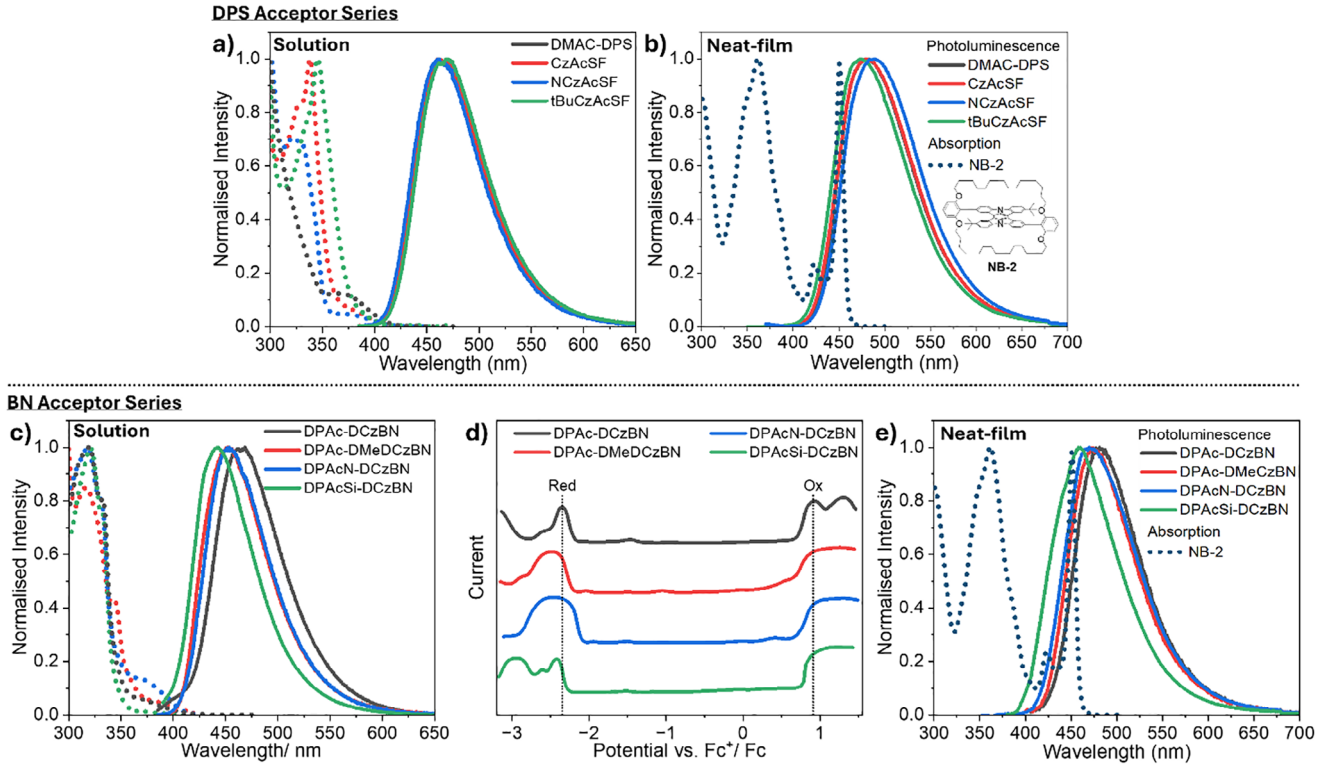

Figure 2. Pertinent photophysical and electrochemical data for the new TADF hosts. a) Absorbance and photoluminescence spectra for the DPS acceptor series in toluene; b) Photoluminescence spectra for the DPS acceptor series in neat film; c) Absorbance and photoluminescence spectra for the BN acceptor series in toluene; d) Differential pulse voltammograms recorded for the BN acceptor series in THF 0.1 M $TBAPF_6$; e) Photoluminescence spectra for the BN acceptor series in neat film.

to blue-shift the emission of **DPAc-DCzBN** by either weaking or strengthening the primary and ancillary donors, respectively (Figure 1e). This afforded the BN acceptor series, which was similarly synthesized by sequential Buchwald–Hartwig and S_NAr chemistry and constitutes **DPAc-DMeDCzBN**, **DPAcSi-DCzBN**, **DPAcN-DCzBN**. We note that this is the first report of the DPAcN donor, which was designed as a more electron-deficient analog of DPAc. The placement of the pyridine nitrogen *ortho* to the sterically shielding spiro junction is expected to have minimal effect on intermolecular interactions.

The new TADF materials were investigated in solution and neat film. In toluene solution the PL spectral profiles of the compounds in the DPS acceptor series are very similar with peak wavelengths (λ_{max}PL) ≈465 nm (**Figure** 2a). The oxidation and reduction potentials for the DPS series recorded in solution by cyclic voltammetry (CV) are also roughly equivalent, particularly considering the experimental error introduced because of poor electrochemical reversibility (Figure S2, Supporting Information). In the neat film the PL spectra are red-shifted compared to the solution, with more pronounced differences in λ_{max}PL across the series (Figure 2b). The neat film emission increases in energy with the ancillary donor strength, affording a λ_{max}PL of 473 nm for **tBuCzAcSF** (vs 479 nm for **DMAC-DPS**). The blue-shifted neat-film emission of **tBuCzAcSF** should be beneficial for promoting FRET to terminal emitters, which is emphasized by its improved spectral overlap with the toluene solution (dispersed) absorption spectrum of **NB-2** compared to **DMAC-DPS** (Figure 2b). **NB-2** is a BT.2020 terminal emitter which we selected based on its established high efficiency in MFHF devices.[20] While **NB-2** displays multi-resonance spectral features with an ultranarrow emission spectrum, it cannot triplet harvest so an efficient TADF host is essential.[20]

The differences in the toluene solution PL spectra are more pronounced for the BN acceptor series (Figure 2c). The emission spectra of **DPAc-DMeDCzBN** and **DPAcN-DCzBN** are each blue-shifted to a λ_{max}PL of 453 nm (vs 465 nm for **DPAc-DCzBN**). Modification to **DPAcSi-DCzBN** pushes the emission to even higher energy (λ_{max}PL = 442 nm). While the electrochemical oxidation and reduction processes of the BN series occur at quite similar potentials, the resolution offered by differential pulse voltammetry (DPV) affords some insight into the origin of the spectral shifts and verifies the design strategies (Figure 2d). Modification of **DPAc-DCzBN** to **DPAc-DMeDCzBN** primarily increases the electrochemical bandgap by weakening the BN acceptor and pushing the reduction to a more negative potential, in line with the increased electron-donating ability of the 3,6-dimethylcarbazole ancillary donors. In contrast, the oxidation potentials of **DPAcN-DCzBN** and **DPAcSi-DCzBN** are both subtly pushed to more positive potentials than that of **DPAc-DCzBN** because of their weaker primary donors. We also note that **DPAcSi-DCzBN** displays a more negative reduction potential than **DPAc-DCzBN**. For the BN acceptor series, the neat-film emission spectra display a similar trend to the solution, with all new compounds displaying higher energy emission than **DPAc-DCzBN**

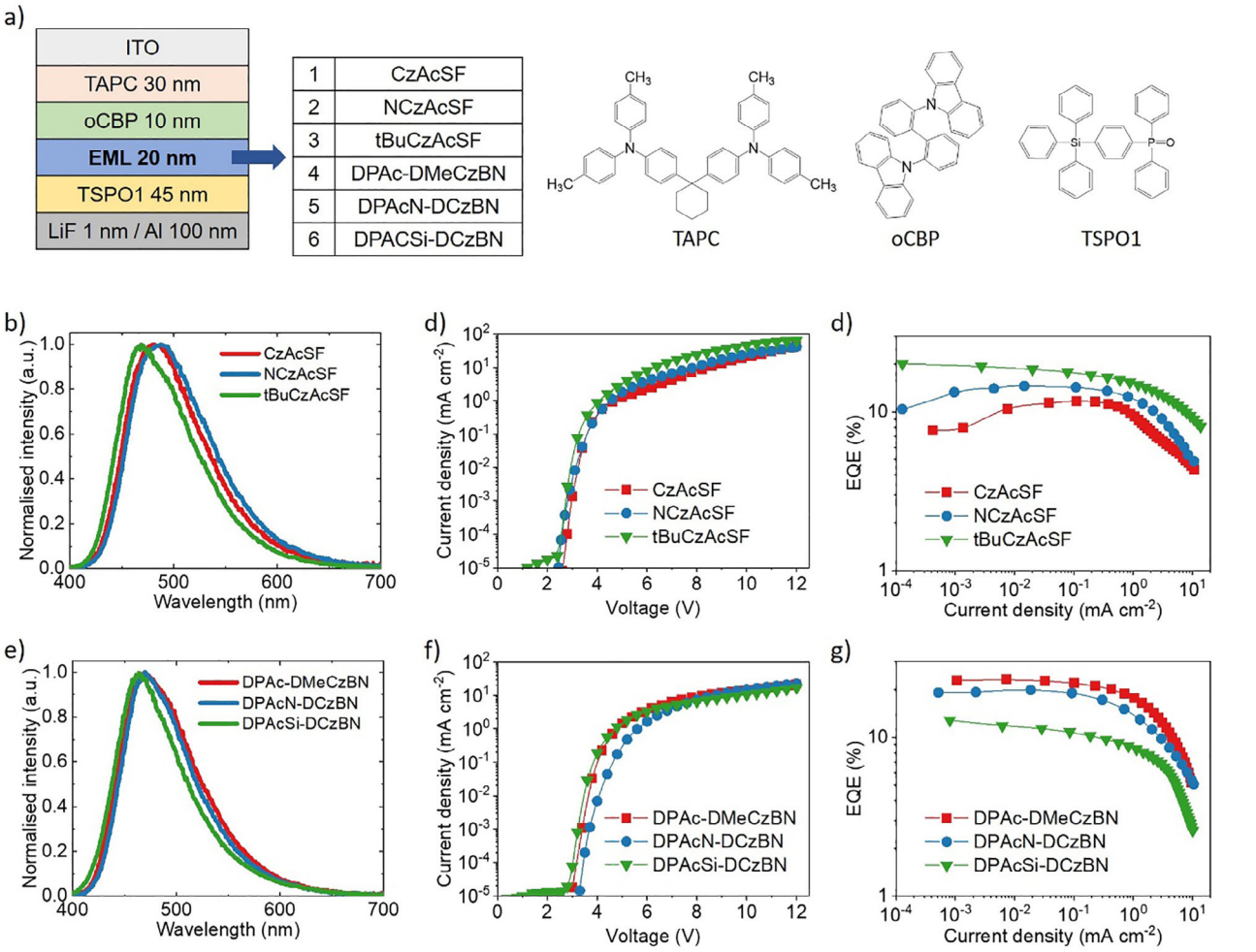

Figure 3. Optoelectronic performance of non-doped TADF OLEDs. a) Device structure with different non-doped TADF materials consisting of the EML and chemical structures for charge transporting layers. b,e) EL spectra at 1 mA cm^{-2}. d,f) Current density–voltage plots. d,g) EQE-current density plots.

(Figure 2e). We note that **DPAcSi-DCzBN** displays a shoulder peak on the blue edge of the neat-film PL spectrum, which could possibly be attributed to conformer effects previously reported for the DPAcSi donor.[30–34]

2.2. Non-Doped Blue TADF OLEDs

All the new materials exhibit the high thermal stability necessary to fabricate OLEDs by thermal evaporation, thermally decomposing ≥350 °C (Figure S1, Supporting Information). Non-doped TADF OLEDs were fabricated with the device structure shown in **Figure 3a**. 1,1-bis[(di-4-tolylamino)phenyl]cyclohexane (TAPC) and 2,2′-di(9H-carbazol-9-yl)-1,1′-biphenyl (oCBP) constitute a hole transport layer (HTL) part, and diphenyl[4-(triphenylsilyl)phenyl]phosphine oxide (TSPO1) is employed for an electron transport layer (ETL). Figure 3b–g shows the device performance of non-doped TADF OLEDs, and they are summarized in **Table 1**.

Regarding the DPS acceptor series, the non-doped **tBuCzAcSF** device exhibits a maximum EQE of 20.1%, which is a greater than 70% improvement compared to the non-doped **CzAcSF** device. Simultaneously, a 12 nm blue-shifted electroluminescence (EL) spectrum leads to a decrease in CIE_y from 0.322 to 0.266. Although the **NCzAcSF** non-doped device shows a higher EQE than the non-doped **CzAcSF** device, its 8 nm red-shifted EL spectrum is not favorable for blue devices. We note that the higher maximum EQE and improved efficiency roll-off of **tBuCzAcSF** compared to **DMAC-DPS** is observed in spite of a slightly decreased PL quantum yield (Φ_{total}) and longer prompt (τ_p) and delayed (τ_d) PL lifetimes. Therefore, the effect of device-specific factors such as carrier balance may contribute to the varying performance of the DPS series.

For the BN acceptor series, non-doped devices fabricated with **DPAcN-DCzBN** and **DPAc-DMeDCzBN** both display impressively high EQEs of more than 20% with CIE_y of ≈0.26. In a non-doped device, **DPAcSi-DCzBN** displays the highest energy emission of all the new hosts, with $CIE_y = 0.214$. While the maximum EQE of **DPAcSi-DCzBN** is the lowest in the BN acceptor series at 12.9%, we note that this value is still higher than for **CzAcSF** with a > 0.1 reduction in CIE_{xy}.

Table 1. Summary of the device performance for non-doped TADF OLEDs.

	V_{on} [a] [V]	EQE_{Max} [%]	V_{100} [b] [V]	EQE_{100} [b] [%]	λ_{peak} [nm]	FWHM [nm]	CIE [x,y]
DMAC-DPS[c]	2.7	17.0	3.3	15.8	476	88.2	0.185, 0.315
CzAcSF	2.8	11.7	4.0	11.1	481	87.1	(0.188, 0.322)
NCzAcSF	2.6	14.6	4.0	13.7	488	90.7	(0.201, 0.356)
tBuCzAcSF	2.6	20.1	3.6	16.7	469	82.5	(0.174, 0.266)
DPAc-DCzBN[c]	2.9	20.3	4.4	18.7	476	86.3	(0.186, 0.313)
DPAcN-DCzBN	3.4	20.0	5.0	17.1	470	76.2	(0.171, 0.259)
DPAcSi-DCzBN	3.0	12.9	4.5	9.0	464	74.0	(0.169, 0.214)
DPAc-DMeCzBN	3.1	23.2	4.2	21.0	469	84.3	(0.175, 0.263)

[a] Voltage at 0.01 cd m^{-2}; [b] Values at 100 cd m^{-2}; [c] Values from ref.[20]

tBuCzAcSF and **DPAc-DMeDCzBN** are the champion materials within their respective series. Therefore, within the limitations of our series, it appears that additional steric bulk is beneficial.

Non-doped **tBuCzAcSF** and **DPAc-DMeDCzBN** devices show similar EL profiles with peak wavelengths of 469 nm and $CIE_{x,y}$ of (0.175, 0.263) and (0.174, 0.266), respectively, which are blue-shifted compared to **DMAC-DPS** and **DPAc-DCzBN**.[20] We note that **DPAc-DMeDCzBN** displays a very high EQE of 23.2% without a host matrix, which can be ranked as one of the highest reported EQEs for a blue non-doped TADF OLED.[22–25,27–29,35] **tBuCzAcSF** also displays a high EQE of 20.1%, which is greater than that recently obtained in our group for **DMAC-DPS** (17.0%) from the same device structure.

The photophysical properties of the higher-performing BN acceptor series were further investigated in neat films to explain the device's performance. The data are summarised in **Table 2** and the PL decays are shown in Figure S4 (Supporting Information). The champion material **DPAc-DMeDCzBN** displays shorter τ_p and τ_d than the parent **DPAc-DCzBN** without any compromise to Φ_{total}, in line with the improved device performance of **DPAc-DMeDCzBN**, particularly the improved efficiency roll-off. **DPAcN-DCzBN** and **DPAcSi-DCzBN** display lower Φ_{total} values. Therefore, the trend in non-doped OLED performance in the BN acceptor series can be rationalized from the neat film photophysical data.

2.3. Pure Blue MFHF OLEDs

Next, MFHF OLEDs were fabricated from the same device structure shown in Figure 3a. The ultranarrow multi-resonance emitter, **NB-2**,[20] was dispersed into the efficient blue TADF hosts **tBuCzAcSF** (**MFHF 1**) and **DPAc-DMeDCzBN** (**MFHF 2**) at 1 wt.% doping. **Figure 4a** shows the EL spectra of the new devices with inset photographs of the devices in operation. The performance of **MFHF 1** and **MFHF 2** are summarised in **Table 3** with reference devices in the parent **DMAC-DPS** and **DPAc-DCzBN** hosts for comparison. Pure blue emission was recorded from both **MFHF 1** and **MFHF 2** with the ultranarrow FWHM of ≤ 15 nm at a peak wavelength of 456 nm. The corresponding chromaticity coordinates were $CIE_{x,y}$ = (0.155, 0.150) for **MFHF 1** and $CIE_{x,y}$ = (0.161, 0.157) for **MFHF 2**. Figure 4b,c show the device characteristics for the new MFHF devices. Maximum EQEs of 19.5% and 22.2% were achieved from **MFHF 1** and **MFHF 2**, respectively, without the support of a host matrix. The Maximum EQEs of **MFHF 1** and **MFHF 2** are only slightly reduced compared to the parent non-doped devices, in line with previous findings where **NB-2** was found to substantially suppress loss through Dexter energy transfer (DET) to the terminal emitter triplet state. Compared to devices using **DMAC-DPS** and **DPAc-DCzBN** as hosts, higher[20] EQEs, narrower FWHM, and bluer $CIE_{x,y}$ values were achieved for the new MFHF devices, correlating with the improved performance (higher energy emission and higher non-doped EQE) of the new blue TADF host materials. We consider this to be substantial progress on MFHF EL devices, which could be a promising strategy to realize high-performing pure blue OLEDs using a simple two-component emissive system that has already been adopted in OLED display products. We also note that while the maximum EQE was lower (11.2%), a further improvement in CIE_{xy} can be afforded when **DPAcSi-DCzBN** is used as the TADF host (0.146, 0.113) (Figure S7 and Table S5, Supporting Information).

Table 2. Summary of the neat film photophysical data for the BN series.

Film	Φ_{total}	Φ_p	Φ_d	τ_p [10^{-9} s]	τ_d [10^{-6} s]	$k_{r,p}$ [10^7 s^{-1}]	$k_{r,d}$ [10^5 s^{-1}]
DPAc-DCzBN[a]	0.91	0.40	0.51	17.0	6.8	2.33	0.76
DPAcN-DCzBN	0.73	0.32	0.41	11.3	4.7	2.81	0.88
DPAcSi-DCzBN	0.55	0.29	0.26	9.60	3.9	3.03	0.67
DPAc-DMeDCzBN	0.92	0.40	0.52	12.5	5.0	3.19	1.05

[a] Values from ref. [20]

2.4. Solid-State Photophysics

Solid-state photophysical studies were conducted to help understand the energy transfer and exciton decay kinetics in the TADF and HF emissive systems that are schematically displayed in **Figure 5a**. In TADF, reversible intersystem crossing between singlet and triplet excited states enables effective triplet harvesting resulting in an IQE of 100% in devices. For high efficiency in HF, excitons should be transferred to the fluorescent terminal emitter through FRET while DET should ideally be completely excluded. In our MFHF system, high efficiency can be achieved as DET is effectively suppressed by the steric protection afforded by alkyl

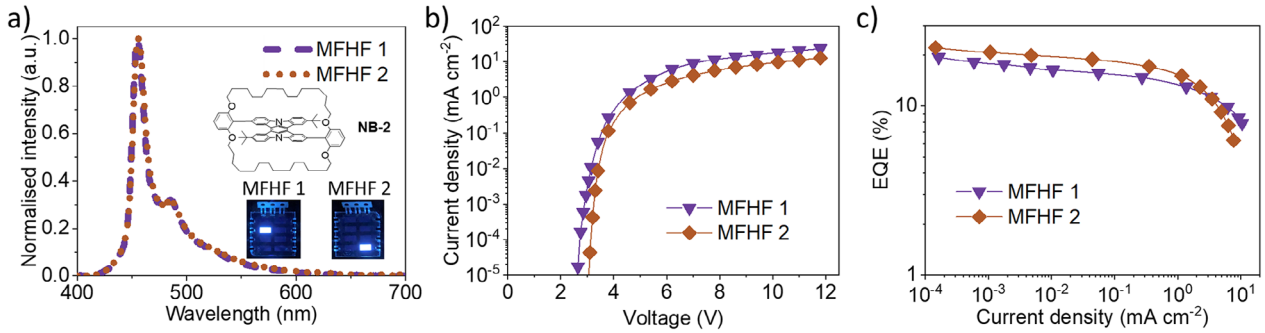

Figure 4. Optoelectronic performance of MFHF OLEDs. a) EL spectra of the devices with the chemical structure of **NB-2**. The inset photos show the device's operation. b) Current density–voltage plots. c) EQE-current density plots for the devices.

Table 3. Summary of the device performance for MFHF OLEDs.

	V_{on} [a] [V]	EQE_{Max} [%]	$V_{1.0}$ [b] [V]	EQE_{100} [b] [%]	λ_{peak} [nm]	FWHM [nm]	CIE [x,y]
MFHF 1	2.7	19.5	4.1	14.2	456	14.4	(0.155, 0.150)
DMAC-DPS:NB-2[c]	2.6	15.6	3.5	14.5	456	15.2	(0.172, 0.191)
MFHF 2	3.1	22.2	4.3	16.9	456	15.0	(0.161, 0.157)
DPAc-DCzBN:NB-2[c]	3.0	21.5	4.4	17.8	458	15.4	(0.161, 0.186)

[a] Voltage at 0.01 cd m^{-2}; [b] Values at 100 cd m^{-2}; [c] Values from ref. [20]

straps.[20] Figure 5b shows the steady-state PL spectra for pristine **tBuCzAcSF** and **DPAc-DMeDCzBN** films with the absorption coefficient profile for **NB-2** (diluted in toluene). The singlet emission of **tBuCzAcSF** and **DPAc-DMeDCzBN** sufficiently covers the strong 0–0 absorption peak of **NB-2**, enabling effective FRET from them to **NB-2**.

To investigate exciton decay kinetics and energy transfer, transient PL measurements were performed for the pristine and **NB-2** doped films. Figure 5c,d show the transient PL profiles for **tBuCzAcSF**- and **DPAc-DMeDCzBN**-based films with and without the **NB-2** dopant. In the non-doped TADF transient PL plots, we observe exciton decay kinetics typical of efficient TADF

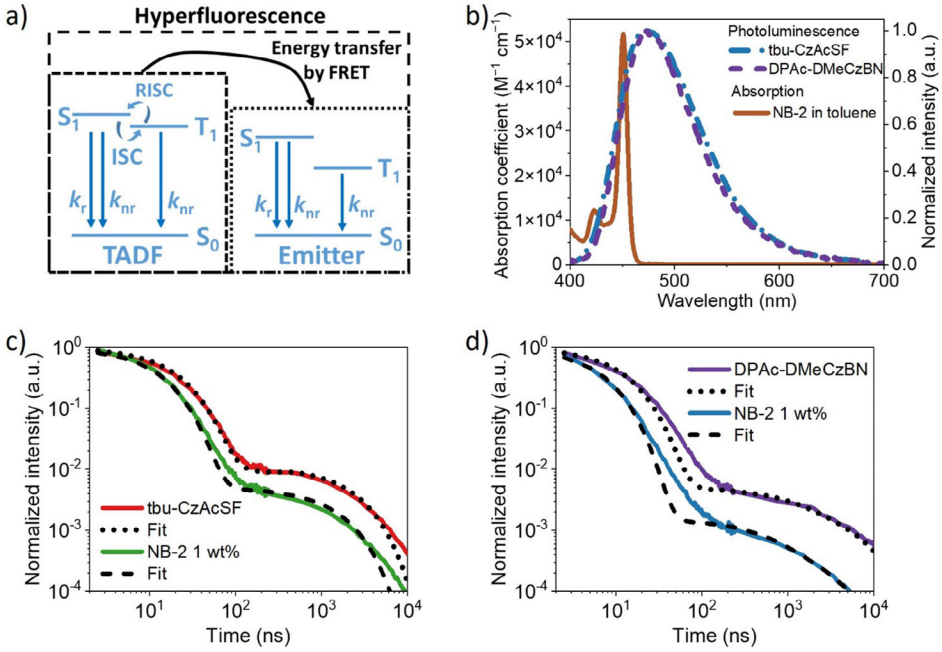

Figure 5. Hyperfluroescence mechanism and photophysical properties. a) Schematic diagram of energy transfer and exciton decay kinetics in hyperfluorescence emissive system. b) Photoluminescence spectra for pristine tbu-CzAcSF and DPAc-DMeCzBN films and absorption spectrum for NB-2. c,d) Transient photoluminescence plots for tbu-CzAcSF and tbu-CzAcSF:NB-2 1 wt.% with bi-exponential fits and DPAc-DMeCzBN and DPAc-DMeCzBN:NB-2 1 wt.% with tri-exponential fits.

materials. Nanosecond-scale exciton decay (19.5 ns for pristine **tBuCzAcSF** and 12.5 ns for pristine **DPAc-DMeDCzBN**) is observed from prompt fluorescence, followed by distinct delayed emission with a microsecond-scale decay (2.3 µs for pristine **tBuCzAcSF** and 5.0 µs for pristine **DPAc-DMeDCzBN**). In the **NB-2**-doped films, faster PL decays are recorded compared to the non-doped TADF films. As a consequence of the short ≈5 ns intrinsic fluorescence time of **NB-2**,[20] efficient FRET to **NB-2** followed by terminal emitter fluorescence offers a faster radiative exciton harvesting pathway than relying on direct $S_1 \rightarrow S_0$ emission from the TADF host.

Meanwhile, the shape of the transient PL profiles for the **NB-2** doped films follow the non-doped TADF films but with faster prompt and delayed decay characteristics, supporting HF energy transfer pathways: 1) prompt FRET and 2) ISC → RISC → delayed FRET. Table S3 (Supporting Information) shows the summary of the steady-state and transient photophysical properties of the relevant non-doped and MFHF OLEDs with pertinent rates. From the steady-state and transient photophysical data, FRET and DET rate constants can be estimated (Table S4, Supporting Information). Owing to the improved PL-absorption overlap between the TADF hosts and **NB-2**, longer Förster radii, faster FRET rates, and higher FRET efficiency were observed at 1 wt.% doping than the values that are reported in our previous work.[20] which led to more efficient and purer blue EL at the same doping concentration. For example, FRET from **DPAc-DMeDCzBN** to **NB-2** is 70% faster than when the parent **DPAc-DCzBN** is used as the host. While the improved non-doped OLED performance and spectral overlap of the new TADF hosts afford substantial progress in MFHF, we note that spectral deconvolution indicates energy transfer to still be incomplete (FRET efficiency ≈65% – Table S4, Supporting Information), highlighting an opportunity for further optimization to achieve even higher performance.

3. Conclusion

New highly efficient blue TADF host materials have been developed and applied to MFHF OLEDs. High EQEs of >23% were realized from non-doped TADF devices with deep blue emission. Leveraging the new TADF hosts in MFHF OLEDs to sensitize an ultranarrow multi-resonance emitter afforded comparable EQEs of >22% while speeding up radiative exciton harvesting and pushing the emission into the pure blue with ultranarrow bandwidth (FWHM ≤ 15 nm and CIE_y ≈0.15). Time-resolved photoluminescence experiments linked the high MFHF OLED performance to the intrinsic high non-doped TADF EQEs of the TADF hosts and effective energy transfer to an encapsulated terminal emitter exhibiting unity PLQE and ultranarrow emission. This work showcases the high potential of matrix-free devices to match and even exceed the performance and stability of matrix-containing hyperfluorescent devices. We show that a promising direction for future research is to focus on the development of improved non-doped deep blue TADF hosts to enable MFHF devices with state-of-the-art performance and stability.

4. Experimental Section

Synthesis, Characterization, and Calculations: The details are described in the Supporting Information.

Sample Preparation: Organic films were made by a thermal evaporation process under high vacuum (≈10^{-7} torr). 30 nm thick neat films were thermally evaporated on glass substrates to measure steady-state PL, PLQE, and transient PL. For the fabrication of OLED devices, ITO-coated substrates (≈15 Ω cm^{-2}) were cleaned with acetone and isopropyl alcohol, and then O_2 plasma treatment was applied to align the energy level with a hole transporting layer. All layers, including organic layers and a LiF/aluminum cathode, were thermally deposited in a high vacuum (≈10^{-7} torr). Here, doping concentrations applied in films and devices were weight percentages.

Photophysical Measurements and Device Characterization: Steady-state PL spectra were measured from an FLS980 spectrofluorimeter with a monochromated xenon arc lamp at λ_{Ex} = 370 nm. Shimadzu UV-3600 Plus spectrophotometer was employed for the measurement of absorption spectra. FLS980 with an integrating sphere under a nitrogen flow was used to measure PLQE, and the films were excited by a 330 nm laser. Transient PL was recorded by using an Andor electrically gated intensified charge-coupled device (ICCD) with 350 nm laser excitation; the decay kinetics were obtained from the integration of the total spectrum at each time. The performance of the OLED devices was measured by using a Keithley 2635 source meter and a calibrated Si photodiode. The EL spectra were recorded by an Ocean Optics Flame spectrometer.

Supporting Information

Supporting Information is available from the Wiley Online Library or from the author.

Acknowledgements

H.-H.C. and D.G.C. contributed equally to this work. R.H.F and H.-H.C. acknowledged the funding from the European Union's Horizon 2020 research and innovation programme (grant agreement number 101020167). D.G.C. acknowledged the Herchel Smith fund for an early career fellowship and the Royal Society (URF\R1\241806). H.B. acknowledged the EPSRC programme grant EP/W017091/1. Prof. Charlotte J. Williams (University of Oxford Chemistry) is acknowledged for the use of their group's equipment for thermal analysis.

Conflict of Interest

The authors declare no conflict of interest.

Data Availability Statement

The data that support the findings of this study are available from the corresponding author upon reasonable request.

Keywords

blue OLED, energy transfer, matrix-free hyperfluorescence, TADF

Received: January 22, 2025
Revised: April 11, 2025
Published online:

[1] C. W. Tang, S. A. Vanslyke, *Appl. Phys. Lett.* **1987**, *51*, 913.
[2] M. A. Baldo, S. Lamansky, P. E. Burrows, M. E. Thompson, S. R. Forrest, *Appl. Phys. Lett.* **1999**, *75*, 4.

[3] M. A. Baldo, D. F. O'Brien, Y. You, A. Shoustikov, S. Sibley, M. E. Thompson, S. R. Forrest, *Nature* **1998**, *395*, 151.
[4] A. Endo, K. Sato, K. Yoshimura, T. Kai, A. Kawada, H. Miyazaki, C. Adachi, *Appl. Phys. Lett.* **2011**, *98*, 083302.
[5] H. Uoyama, K. Goushi, K. Shizu, H. Nomura, C. Adachi, *Nature* **2012**, *492*, 234.
[6] H. Nakanotani, T. Higuchi, T. Furukawa, K. Masui, K. Morimoto, M. Numata, H. Tanaka, Y. Sagara, T. Yasuda, C. Adachi, *Nat. Commun.* **2014**, *5*, 4016.
[7] T. Furukawa, H. Nakanotani, M. Inoue, C. Adachi, *Sci. Rep.* **2015**, *5*, 8429.
[8] R. Braveenth, H. Lee, J. D. Park, K. J. Yang, S. J. Hwang, K. R. Naveen, R. Lampande, J. H. Kwon, *Adv. Funct. Mater.* **2021**, *31*, 2105805.
[9] J. H. Kim, K. H. Lee, J. Y. Lee, *J. Mater. Chem. C* **2020**, *8*, 5265.
[10] S. K. Jeon, H. J. Park, J. Y. Lee, *ACS Appl. Mater. Interfaces* **2018**, *10*, 5700.
[11] D. Zhang, X. Song, A. J. Gillett, B. H. Drummond, S. T. E. Jones, G. Li, H. He, M. Cai, D. Credgington, L. Duan, *Adv. Mater.* **2020**, *32*, 1908355.
[12] D. Li, Y. Hu, L. S. Liao, *J. Mater. Chem. C* **2019**, *7*, 977.
[13] S. H. Han, J. H. Jeong, J. W. Yoo, J. Y. Lee, *J. Mater. Chem. C* **2019**, *7*, 3082.
[14] D. Zhang, X. Song, M. Cai, L. Duan, *Adv. Mater.* **2018**, *30*, 1705250.
[15] D. H. Ahn, J. H. Jeong, J. Song, J. Y. Lee, J. H. Kwon, *ACS Appl. Mater. Interfaces* **2018**, *10*, 10246.
[16] C. Y. Chan, M. Tanaka, Y. T. Lee, Y. W. Wong, H. Nakanotani, T. Hatakeyama, C. Adachi, *Nat. Photonics* **2021**, *15*, 203.
[17] S. O. Jeon, K. H. Lee, J. S. Kim, S. G. Ihn, Y. S. Chung, J. W. Kim, H. Lee, S. Kim, H. Choi, J. Y. Lee, *Nat. Photonics* **2021**, *15*, 208.
[18] H. H. Cho, A. S. Romanov, M. Bochmann, N. C. Greenham, D. Credgington, *Adv. Opt. Mater.* **2021**, *9*, 2001965.
[19] S. G. Ihn, N. Lee, S. O. Jeon, M. Sim, H. Kang, Y. Jung, D. H. Huh, Y. M. Son, S. Y. Lee, M. Numata, H. Miyazaki, R. Gómez-Bombarelli, J. Aguilera-Iparraguirre, T. Hirzel, A. Aspuru-Guzik, S. Kim, S. Lee, *Adv. Sci.* **2017**, *4*, 1600502.
[20] H. H. Cho, D. G. Congrave, A. J. Gillett, S. Montanaro, H. E. Francis, V. Riesgo-Gonzalez, J. Ye, R. Chowdury, W. Zeng, M. K. Etherington, J. Royakkers, O. Millington, A. D. Bond, F. Plasser, J. M. Frost, C. P. Grey, A. Rao, R. H. Friend, N. C. Greenham, H. Bronstein, *Nat. Mater.* **2024**, *23*, 519.
[21] D. Zhang, L. Duan, C. Li, Y. Li, H. Li, D. Zhang, Y. Qiu, *Adv. Mater.* **2014**, *26*, 5050.
[22] Y. Z. Shi, H. Wu, K. Wang, J. Yu, X. M. Ou, X. H. Zhang, *Chem. Sci.* **2022**, *13*, 3625.
[23] J. Han, Z. Huang, J. Miao, Y. Qiu, Z. Xie, C. Yang, *Chem. Sci.* **2022**, *13*, 3402.
[24] Z. Zhang, D. Dou, R. Xia, P. Wu, E. Spuling, K. Wang, J. Cao, B. Wei, X. Li, J. Zhang, S. Bräse, Z. Wang, *Sci. Adv.* **2023**, *9*, adf4060.
[25] S. J. Zou, F. M. Xie, M. Xie, Y. Q. Li, T. Cheng, X. H. Zhang, C. S. Lee, J. X. Tang, *Adv. Sci.* **2020**, *7*, 1902508.
[26] W. Song, I. Lee, J. Y. Lee, *Adv. Mater.* **2015**, *27*, 4358.
[27] H. J. Tan, J. R. Yu, Z. Z. Lin, G. X. Yang, Z. Q. Long, Y. L. Deng, Z. L. Zhu, X. K. Chen, J. X. Jian, Q. X. Tong, C. S. Lee, *Chem. Eng. J.* **2024**, *481*, 148567.
[28] Q. Zhang, D. Tsang, H. Kuwabara, Y. Hatae, B. Li, T. Takahashi, S. Y. Lee, T. Yasuda, C. Adachi, *Adv. Mater.* **2015**, *27*, 2096.
[29] Z. Cheng, Z. Li, Y. Xu, J. Liang, C. Lin, J. Wei, Y. Wang, *ACS Appl. Mater. Interfaces* **2019**, *11*, 28096.
[30] I. S. Park, H. Min, J. U. Kim, T. Yasuda, *Adv. Opt. Mater.* **2021**, *9*, 2101282.
[31] M. K. Etherington, F. Franchello, J. Gibson, T. Northey, J. Santos, J. S. Ward, H. F. Higginbotham, P. Data, A. Kurowska, P. L. Dos Santos, D. R. Graves, A. S. Batsanov, F. B. Dias, M. R. Bryce, T. J. Penfold, A. P. Monkman, *Nat. Commun.* **2017**, *8*, 14987.
[32] H. J. Tan, G. X. Yang, Y. L. Deng, C. Cao, J. H. Tan, Z. L. Zhu, W. C. Chen, Y. Xiong, J. X. Jian, C. S. Lee, Q. X. Tong, *Adv. Mater.* **2022**, *34*, 2200537.
[33] S. J. Li, X. Tang, C. H. Ng, J. Y. Lim, W. K. Tang, W. C. Chen, Y. Huo, M. Ng, S. S. Chen, D. Zhang, L. Duan, M. C. Tang, *Adv. Opt. Mater.* **2025**, https://doi.org/10.1002/adom.202402479.
[34] K. Matsuo, T. Yasuda, *Chem. Sci.* **2019**, *10*, 10687.
[35] G. Xia, C. Qu, Y. Zhu, J. Ye, K. Ye, Z. Zhang, Y. Wang, *Angew. Chem., Int. Ed.* **2021**, *60*, 9598.